https://doi.org/10.1016/0041-624X(89)90059-0

Precision laser-ultrasonic velocity measurement and elastic constant determination

J.-D. Aussel and J.-P. Monchalin

Industrial Materials Research Institute, National Research Council of Canada, 75 de Mortagne, Boucherville (Quebec), J4B 6Y4, Canada

Received 30 June 1988

A laser-ultrasonic method to measure the acoustic velocities and the elastic constants of solid materials based on the crosscorrelation of successive echoes is presented. Measurements are performed in the thermoelastic regime or slight ablation regime, which permits simultaneous measurement of longitudinal shear velocities and an unlimited number of shots at the specimen. Diffraction corrections are calculated, and dispersion effects are evaluated by frequency analysis. The precision and accuracy of the technique are estimated in terms of sampling rate, thickness of the sample, signal-to-noise ratio, frequency bandwidth and laser-beam alignment. Examples of applications of the technique are given for PZT ceramic, metal–ceramic composites and single crystal germanium.

Keywords: laser ultrasonics; acoustic velocity; elastic constants

New technological needs are leading to the development of new materials with enhanced mechanical properties for specific applications. The knowledge of the elastic properties of these new materials, i.e. the elastic constants, is in practice of great importance. In the case of isotropic materials, two constants have to be determined, either the Lame constants, or the Young's modulus and Poisson's ratio, or the bulk and shear moduli. For an anisotropic material, the measurement of three to twenty one constants, depending on material symmetry, may be needed. Elastic constants are frequently determined nondestructively with acoustical methods[1,2], mainly resonance methods (measurement of longitudinal and torsional resonance frequencies of samples of known geometry) or pulse-echo methods (measurement of compressional and shear ultrasonic velocities with piezoelectric transducers).

Many of these new materials are ceramics or composites of ceramics and are intended for use at elevated temperatures. The measurement of their elastic properties at high temperature is then needed. Variation of the elastic constants with temperature may also provide information on material structure, phase changes and other physical phenomena of interest. Pulse-echo methods are difficult at high temperature[3,4]. They require machining the samples to close tolerances in thickness and surface flatness. Buffer rods, cooling system, special bonds or momentary contact are necessary to keep ultrasonic transducers below their Curie point. Resonance methods have been used successfully at high temperature on various crystals[5]. However they also require proper machining of the samples and proper identification of the resonance peaks is generally very tedious.

These difficulties are solved by the laser-ultrasonic technique which uses lasers to generate and detect ultrasound at a distance, without any contact to the specimen. In this technique a pulsed laser generates ultrasound through thermal expansion at low power densities (thermoelastic effect) or by vaporizing a small amount of surface material at high power densities (ablation effect)[6]. The laser generated ultrasound is detected at the surface of the sample by a second laser coupled to an interferometer[7]. Precise sample machining is not required. This technique has been recently used to measure acoustic velocities in toxic materials[8], high temperature metals[9–11] and ceramic–metal composites[11,12].

One main problem encountered by laser-ultrasonics is the poor signal-to-noise ratio. This is particularly severe for specimens with absorbing and strongly scattering surfaces. The best signal-to-noise ratio is obtained in the ablation regime, which produces longitudinal ultrasonic pulses with amplitudes of the same order of magnitude as conventional ultrasonic transducers. However, this regime has the drawback that a small quantity of material is vaporized at the surface. In many cases of laboratory testing, this small surface damage is acceptable. However, this is not the case if the measurement has to be repeated at the same spot since this could lead to a hole in the specimen. Repeated measurements at the same location are needed for measuring the elastic constants as a function of temperature. In this case the experiment is long and the generating laser is directed onto the sample not only for data acquisition but also to optimize the alignment between the generating and receiving spots on opposite sides of the specimen (single side generation and detection is not generally used to avoid the strong perturbation produced at detection by the plasma generated). Alignment between spots has to be readjusted since lasers generally do not have a sufficient ponting stability. For the same reason, the ablation regime does not allow an increase in the signal-to-noise ratio by averaging.

Another drawback of the ablation regime is the low amplitude of the shear ultrasonic pulses generated, which

0041-624X/89/030165-13 $03.00

makes a precise determination of the shear velocity difficult. Previously reported laser-ultrasonic measurements of elastic constants were performed in the ablation regime, using either longitudinal to shear mode conversion[8] or off-epicentre[11] techniques to assess shear velocity. The mode conversion method requires machining of the sample to a precise special shape (such as a rod) and the off-epicentre method cannot be very accurate since it depends on precise knowledge of the geometrical offset. These works also generally rely on the time of arrival of the first pulse (longitudinal or shear). This time was defined as the time of the beginning of the signal[11,12], which has the consequence that the accuracy is limited by the signal-to-noise ratio, since the beginning of the pulse is contained in the noise. It has also been defined as the time at which the amplitude of the longitudinal pulse reaches an arbitrary level of 10% of his maximum amplitude[9], which leads to a value of velocity that is dependent on the pulse shape. These works based on single pulse recording are also limited by the knowledge of the initial time, i.e. the time taken for the laser pulse to reach the surface. This initial time is affected by the delay introduced by the electronic circuitry and the rise time of the triggering system. Modelling of the pulse shape and least square fit of the experimental data with theoretical data has also been used to measure the arrival time[10]; this method is rather difficult to apply, since it needs accurate knowledge of the generating source (geometrical dimensions and time dependence) and modelling of ultrasonic propagation in the sample, which is in particular difficult in the case of anisotropic samples. This single pulse recording method is acceptable if the absolute value of the velocity is not needed, for example in experiments to monitor phase changes *versus* temperature or in the extreme case where only one pulse, longitudinal or shear, is observed.

The method presented below does not have the limitations mentioned above and permits high accuracy measurement of absolute ultrasonic velocities at ambient or elevated temperatures. Instead of using only the first longitudinal and shear pulses, two consecutive longitudinal and shear echoes are used, as in conventional ultrasonic techniques. The echoes are measured at epicentre, so only the measurement of the thickness of the sample is needed to calculate velocities from times-of-flight. The measurements are performed in the thermo-elastic or slight ablation regime, which permits simultaneous measurement of longitudinal and shear velocities, signal averaging and an unlimited number of shots at the specimen because of the absence of surface damage. A crosscorrelation technique, which is less sensitive to poor signal-to-noise conditions, is used to measure the time delay between successive echoes. Examples of application of the technique are given for a PZT ceramic and metal–ceramic composites. Corrections introduced by ultrasonic diffraction are estimated and dispersion effects are dealt with by frequency analysis of the crosscorrelation function. Accuracy of the technique is tested by comparing the results obtained for a single crystal of germanium to values previously measured by conventional techniques.

Experimental apparatus and typical recorded waveforms

The experimental set-up is shown in *Figure 1*. The generation laser is a pulsed Nd:YAG laser that provides

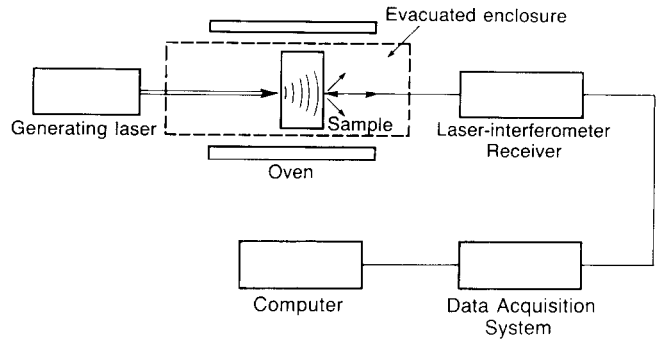

Figure 1 Schematic of the experimental apparatus

10 ns pulses of 0.75 J maximum energy. The generation laser beam is focussed on one side of the sample, and generates an acoustic wave by thermoelastic and/or ablation effect. A variable attenuator is used to set the incident power density in the thermoelastic or slight ablation range. The laser-generated acoustic displacement propagates in the sample and is detected on the opposite face of the sample at the epicentre with a displacement laser-interferometer described previously[13,14]. This interferometer has a bandwidth extending from 250 kHz to 35 MHz. It uses a 1 W single mode cw Argon laser that gives greater sensitivity than the low power HeNe lasers generally used, and makes measurements on scattering surfaces easier. To perform measurements at high temperature, the sample is enclosed in a quartz tube fitted in a tubular oven. The temperature is limited to about 1000°C by softening of quartz. Higher temperatures could be reached with a tube of different material. To avoid oxidation of the specimen, the tube is evacuated to pressures in the range of 10^{-5} torr. Signals are recorded at a sampling rate of 5 ns, stored and processed on a computer.

The samples used as examples in this paper are: a PZT ceramic disc of 22 mm diameter and 6.066 mm thickness with polished planar faces; an Al_2O_3-Al-SiC (No. 1) ceramic–metal composite of 25 mm diameter and 3.249 mm thickness with polished planar faces; an Al_2O_3-Al-SiC (No. 2) ceramic–metal composite sample cut from a tubular engine part of 2.360 mm thickness and unpolished curved faces of 25 mm radius of curvature; an Al_2O_3-Al ceramic–metal composite sample cut from a tubular engine part of 3.800 mm thickness and 25 mm radius of curvature; a single crystal Germanium disc orientated in the ⟨100⟩ direction of 30 mm diameter and 3.167 mm thickness with polished planar faces; and finally a single crystal Germanium disc orientated in the ⟨111⟩ direction of 15 mm diameter and 3.132 mm thickness with polished planar faces. These samples are listed in *Table 1* with corresponding experimental results.

Two typical waveforms obtained from the alumina-aluminum-silicon carbide (Al_2O_3-Al-SiC No. 1) ceramic–metal composite and the PZT ceramic sample are shown in *Figures 2* and *3*, respectively. These data show that the various longitudinal and shear wave arrivals cannot always be easily identified. Since unambiguous identification of the longitudinal and shear pulses is a prerequisite to any velocity measurement, waveforms produced by a theoretical model would be very useful. Such waveforms generated by thermoelastic and ablation mechanisms in isotropic solids are presented below.

Table 1 Summary of the samples used as examples in this paper and the corresponding results

Identification	Al_2O_3-Al-SiC (No. 1)	PZT	Al_2O_3-Al-SiC (No. 2)	Al_2O_3-Al	Ge ⟨100⟩	Ge ⟨111⟩
Data shown in figure	2, 10, 11	3, 7	8	12	13	13
Shape	Planar polished	Planar polished	Curved unpolished	Curved unpolished	Planar polished	Planar polished
Thickness (mm)	3.249	6.066	2.360	3.800	3.167	3.132
Thickness precision (%)	0.08% 2.5 μm	0.04% 2.5 μm	0.4% 10 μm	0.3% 10 μm	0.08% 2.5 μm	0.08% 2.5 μm
Time precision from laser alignment	0.32%	0.04%	0.15%	*L* 0.24% *S* 0.12%	*L* 0.16% *S* 0.12%	*L* 0.17%
Signal-to-noise ratio	*L* 28 dB	*L* 20 dB	*L* 12 dB	*L* 20 dB *S* 10 dB	*L* 40 dB *S* 20 dB	*L* 40 dB
Time standard deviation	0.032/*f* (μs) *f* in MHz	*L* 0.02%	*L* 0.1%	*L* 0.15% *S* 0.20%	*L* 0.02% *S* 0.03%	*L* 0.02%
Precision on time delay measurement	1.0% at 10 MHz	*L* 0.05%	*L* 0.2%	*L* 0.31% *S* 0.23%	*L* 0.16% *S* 0.12%	*L* 0.17%
Diffraction corrections	−0.10%	−0.03%	−0.2%	−0.10%	−0.10%	−0.10%
Dispersion	Resolved	Negligible	Not resolved	Not resolved	Negligible	Negligible
Absolute accuracy of velocity	≈1% at 10 MHz	0.1%	A few % limited by dispersion	A few % limited by dispersion	*L* 0.24% *S* 0.20%	*L* 0.25%

The uncertainty of thickness determination given by the micrometer is 2.5 μm for planar samples and 10 μm for curved samples. Laser beams alignment is assumed to give an uncertainty of 1 ns. The standard time deviation is calculated from equation (10) or (31) and the diffraction correction from equations (21b) and (24b). The precision on time delay is calculated by combining quadratically the alignment time precision and the standard time deviation. The absolute accuracy is deduced from the time delay measurement precision and the uncertainty on the thickness determination

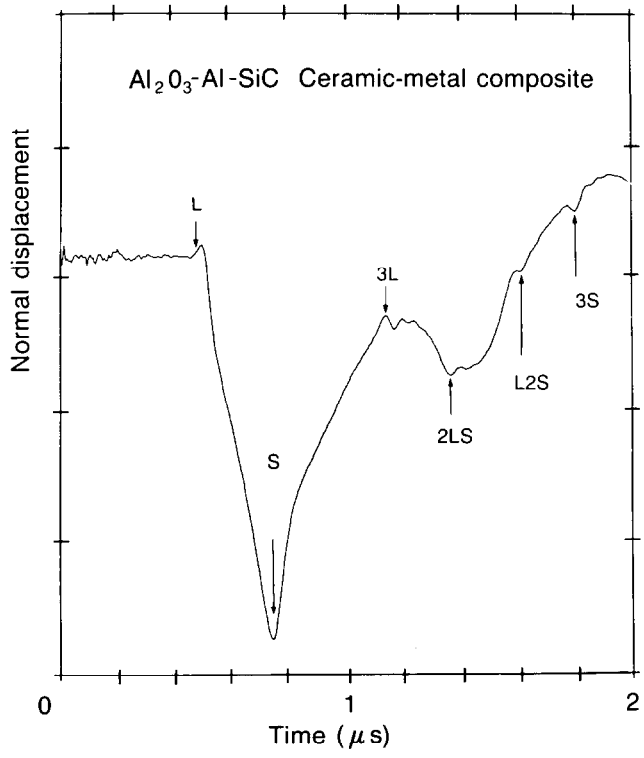

Figure 2 Experimental displacement measured at epicentre on the 3.249 mm thick Al_2O_3-Al-SiC (No. 1) ceramic–metal composite plate. The laser pulse has 10 ns duration and the spot size is ≈0.5 mm in diameter

Laser-generated acoustic waveforms in an isotropic solid

Thermoelastic effect

At low laser power density, the increase in temperature is sufficiently small to avoid any change of state in the material and the elastic stresses generated are caused by thermal expansion. In the case where the heat source is localized on the surface (a small skin depth or a very high absorption coefficient of laser light), the elastic source is known to be equivalent to a horizontal dipole on the surface of steplike time dependence[15]. A typical theoretical waveform at the epicentre, in front of the source on the opposite side, of a plate generated by the thermoelastic mechanism is represented in *Figure 4*. The calculation of the theoretical waveforms has been performed with a computer program developed by Hsu[16]. The generating laser pulse is assumed to have a gaussian time dependence and finite size on the surface. The first longitudinal, *L*, and shear, *S*, arrivals have steplike time dependence. Arrivals after an additional round-trip are denoted 3*L* and 3*S*. Finite dimension of the heated zone causes mode conversion pulses, which are denoted 2*LS*, *L*2*S*, 4*LS*.

Ablation effect

At higher laser power density, the temperature increase is sufficiently high to cause melting and vaporization at the surface and ejection of a small amount of material. The elastic stress generated is essentially caused by this material ejection, so the elastic source is equivalent to a

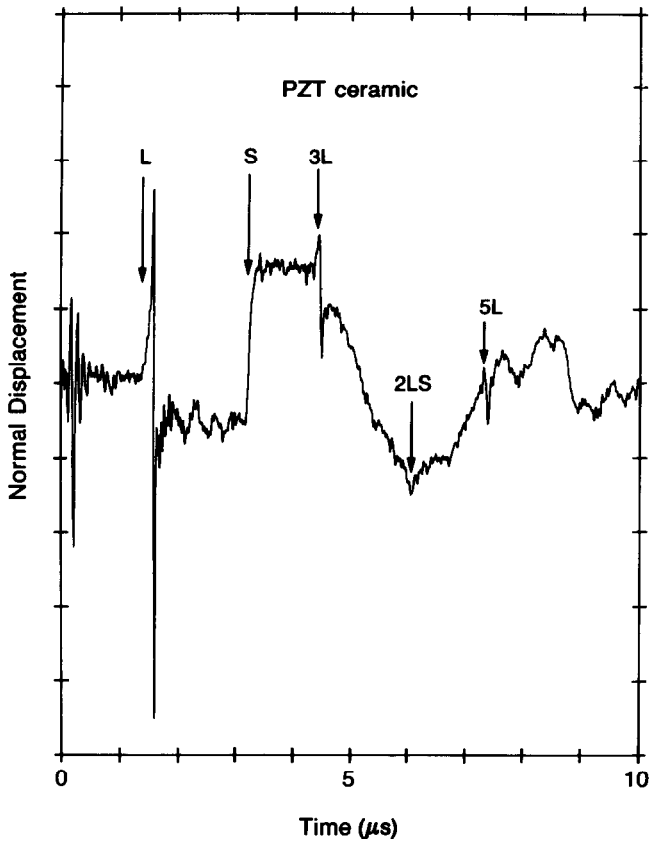

Figure 3 Experimental displacement at epicentre on a 6.066 mm thick PZT ceramic sample. The laser pulse has 10 ns duration and the spot size is ≈0.5 mm in diameter. Initial signal at the beginning of the plot is parasitic and not ultrasonic

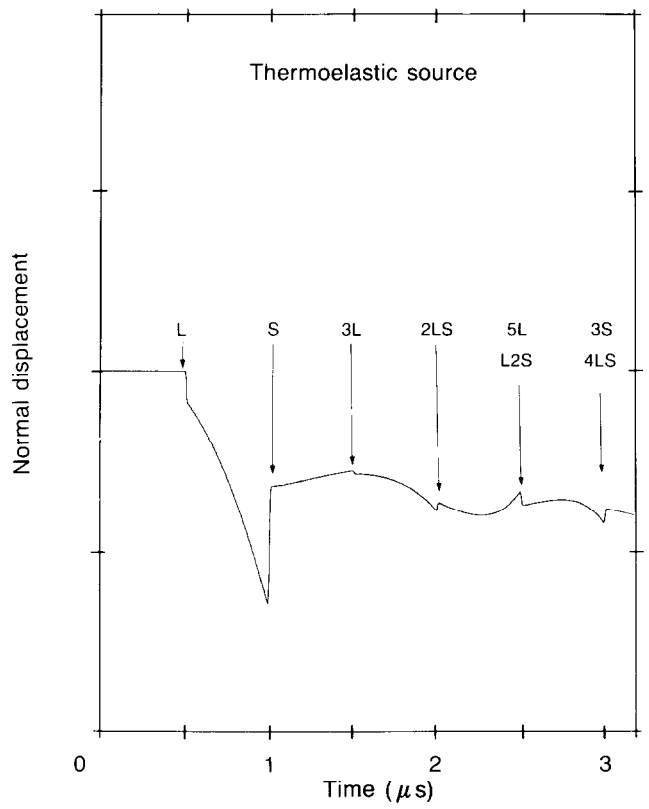

Figure 4 Epicentral normal displacement generated by thermoelastic effect. Laser pulse duration 10 ns; spot diameter 20 μm; plate thickness 3 mm; longitudinal velocity 6 mm μs^{-1}; shear velocity 3 mm μs^{-1}

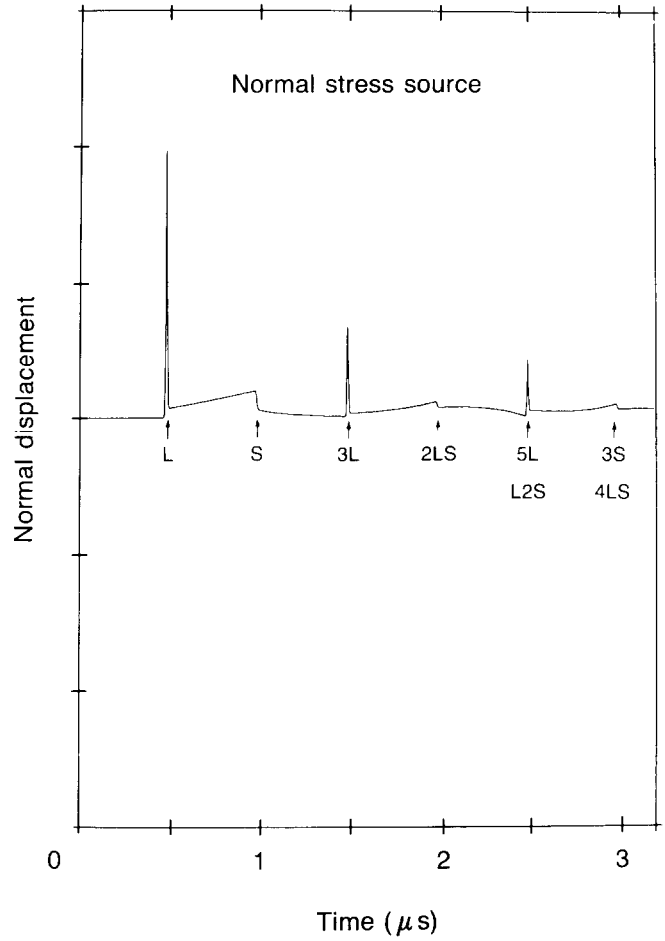

Figure 5 Epicentral normal displacement generated by a normal impulse stress: Laser pulse duration 10 ns; spot diameter 20 μm; plate thickness 3 mm; longitudinal velocity 6 mm μs^{-1}; shear velocity 3 mm μs^{-1}

normal force[6]. If the energy deposited is not too high, the surface cools down rapidly and the force follows a pulse time dependence (at higher energies, a step-like dependence is observed). A typical theoretical waveform at the epicentre produced by a pulsed normal stress is represented in *Figure 5*. The longitudinal wavefront *L* has pulse time dependence, and the shear wavefront is steplike and smaller.

Intermediate regime

At the onset of ablation, ablation and thermoelastic effects have the same order of magnitude and the displacement at the epicentre is a combination of those given in *Figures 4* and *5*. A typical theoretical waveform at the epicentre in the intermediate regime is given in *Figure 6*.

These theoretical results could be useful for identification of the various wave arrivals. For example, the features seen in the theoretical plot, shown in *Figure 6*, can be retrieved in the experimental data of *Figure 2*, with differences originating from a wider generation zone and the low frequency cut-off of the interferometric receiver (≈250 KHz). The data of *Figure 3* is not accurately described by the theoretical model since in this case the material absorbs more weakly and the heat source is distributed underneath the surface. The bipolar aspect of the longitudinal arrival is consistent with previous observations. In the examples presented in *Figures 2* and *3*, the signal-to-noise conditions, as it is often the case

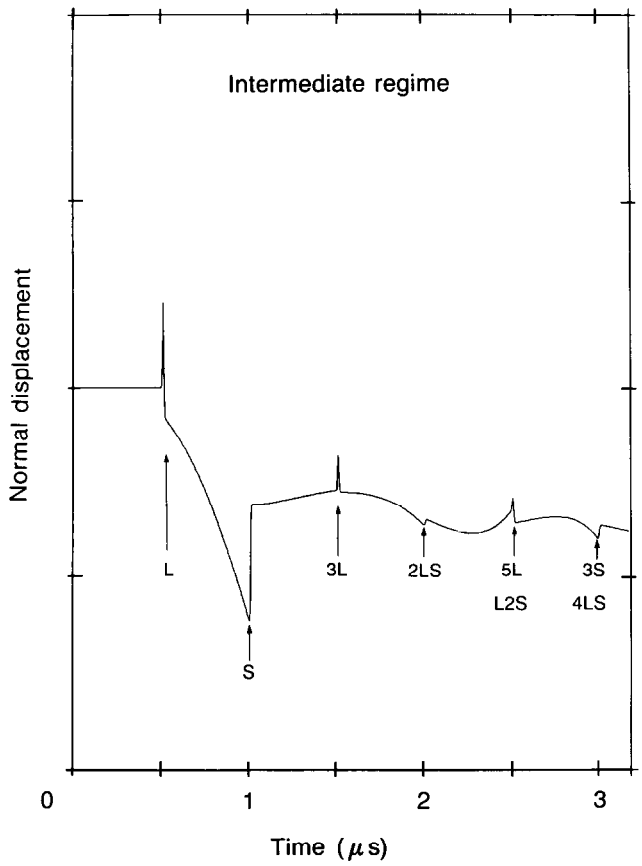

Figure 6 Epicentral normal displacement generated by both thermoelastic and ablation mechanisms: Laser pulse duration 10 ns; spot diameter 20 μm; plate thickness 3 mm; longitudinal velocity 6 mm μs^{-1}; shear velocity 3 mm μs^{-1}

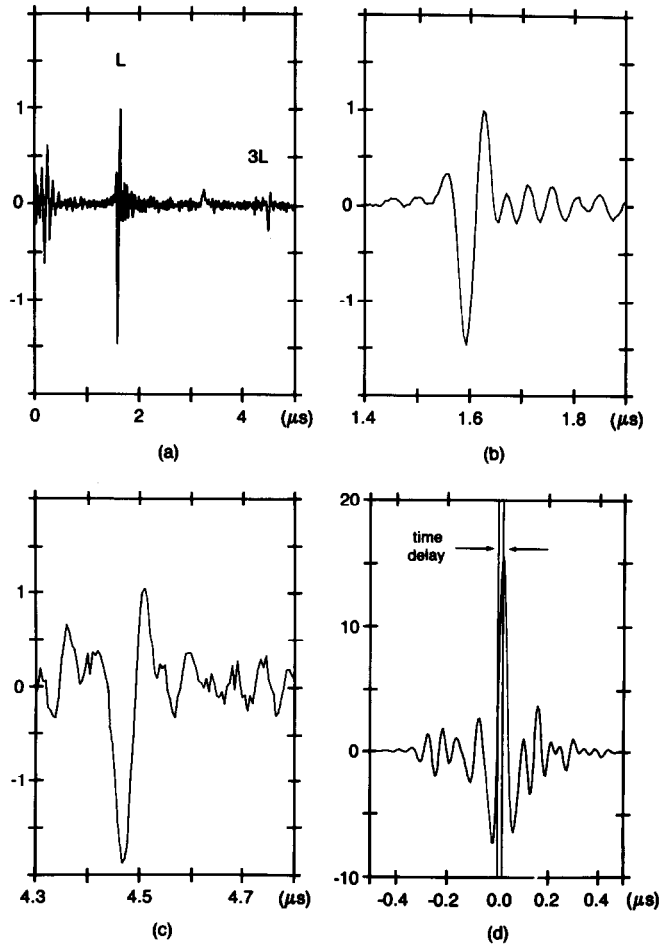

Figure 7 Crosscorrelation measurement of time arrival in the PZT ceramic sample of *Figure 3*. (a) Epicentral particle velocity (derivative of the epicentral displacement of *Figure 3*); (b) normalized and mean value corrected *L* arrival; (c) normalized and mean value corrected 3*L* arrival; (d) crosscorrelation of the two data portion in (b) and (c). The coarse delay is 4.300 – 1.400 = 2.900 μs. The fine delay measured at the maximum of the crosscorrelation is 0.020 μs. Final roundtrip time: $t_{2L} = 2.900 - 0.020 = 2.880$ μs.

with laser-ultrasonics, are not excellent and direct measurement, as it has been done previously[8-12], will lead to very inaccurate values of velocities. A processing technique less sensitive to noise is described below.

Time delay measurement procedure

The procedure used is based on the crosscorrelation of consecutive echoes. Crosscorrelation time delay measurements have been used successfully with conventional pulsed ultrasonic contact techniques[17], giving the most reliable and reproducible results in difficult cases, such as highly attenuating materials, where the reflected echoes 3*L*, 3*S* are very noisy and distorted. The cross-correlation of two time signals $u(t)$ and $v(t)$ is defined by

$$C_{uv}(\tau) = \lim_{T \to \infty} \frac{1}{T} \int_0^T u(t)v(t+\tau)\,dt \qquad (1)$$

The time delay measurement by crosscorrelation is based on the property that the autocorrelation $C_{uu}(\tau)$ of a signal $u(t)$ is an even function of τ, which is maximum at $\tau = 0$. If $v(t)$ is the signal $u(t)$ delayed by T

$$v(t) = u(t - T) \qquad (2)$$

the crosscorrelation function $C_{uv}(\tau)$ will be the autocorrelation $C_{uu}(\tau)$ shifted by T

$$C_{uv}(\tau) = C_{uu}(\tau - T) \qquad (3)$$

and will therefore have its maximum at $\tau = T$.

The procedure to measure time delay between successive reflections is illustrated in *Figure 7* with data taken from *Figure 3* on the PZT ceramic sample. To measure the longitudinal velocity for example, the longitudinal direct arrival *L* and reflected arrival 3*L* are first identified. To eliminate the low frequency component of the signal, we take the derivative of the displacement that gives the particle velocity.

The resulting velocity is shown in *Figure 7a*. The low frequencies could also have been directly eliminated by high-pass filtering or by analogue derivation of the signal. Two portions of the data curve, each including one of these arrivals are then selected by two windows of length T, one starting at time t_1 and the other at time t_2. Both data portions are then normalized to the same energy and their mean value is set to zero (d.c. offset elimination). Normalized and mean value corrected data portions are shown in *Figures 7b* and *c*. The result of crosscorrelation of the two data portions is given in *Figure 7d*. The coarse delay between the two windows is $T_c = t_2 - t_1$. The maximum of the crosscorrelation gives the fine delay, T_f. The round trip time t_{2L} corresponding to the propagation time of the longitudinal pulse over two plate thicknesses is therefore

$$t_{2L} = T_c + T_f \qquad (4)$$

In the case of *Figure 7*, the measured propagation time is 2880 ns, and the calculated velocity is therefore 4212 ms^{-1}. This procedure does not require knowledge of the initial time and the determination of the exact arrival time of the wavefront signals. It uses the whole shape of the wavefront signals, and therefore diminishes the effect of local uncorrelated noise.

The precision of this measurement can be readily evaluated by differentiating the formula $c = x/t$ relating the velocity c to the sample thickness x and the propagation time t

$$\frac{\delta c}{c} = \frac{\delta t}{t} + \frac{\delta x}{x} \tag{5}$$

where δt is the uncertainty on the time measurement, equal to the sampling interval t_s, and δx is the error on the thickness measurement. Applying Equation (5) to the example given above, we find a precision equal to 0.2%. This precision is mostly limited by the sampling time interval, and could be enhanced by using a shorter sampling interval or an interpolation technique, such as the one described below.

Time delay resolution enhancement using interpolation and precision of the crosscorrelation method

The limitations introduced by the sampling interval are illustrated by the data shown in *Figure 8*, which was obtained with the Al_2O_3-Al-SiC (No. 2) ceramic–metal composite, and which shows the variation of its longitudinal velocity with temperature. The sample had a thickness of 2.360 mm and was cut from a tube. This measurement illustrates in particular the ability of the laser-ultrasonic technique to operate on nonplanar samples. The data shown by the open circles and which were obtained by crosscorrelation show several steps. These steps are caused by the 5 ns limited sampling resolution and correspond to successive arrival times, multiples of the 5 ns sampling interval.

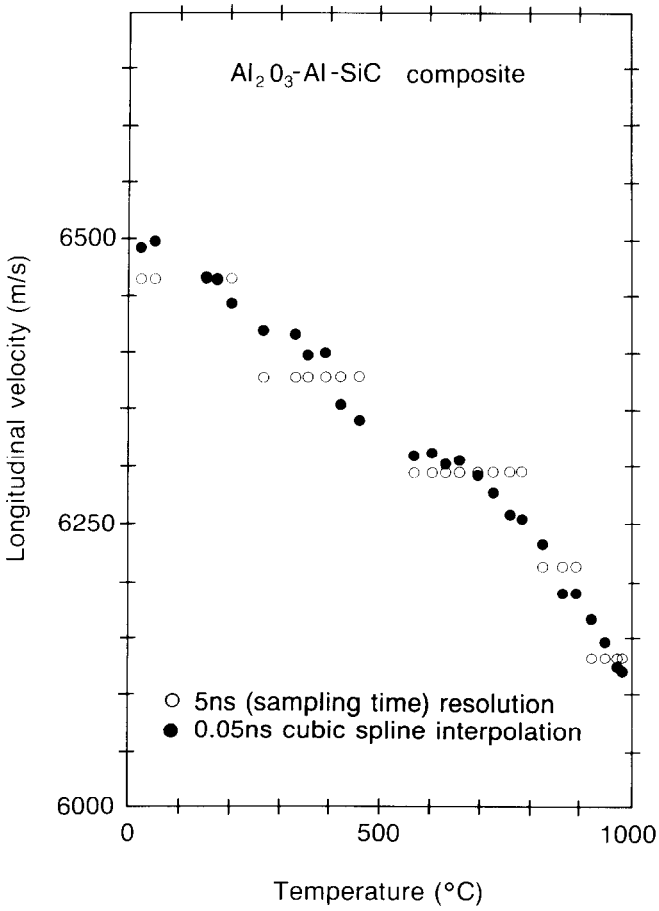

Figure 8 Enhancement of the precision of the time delay measurement by interpolation. The sample is the 2.360 mm thick Al_2O_3-Al-SiC (No. 2) ceramic–metal composite

Sampling time limitations can be minimized by using an interpolation algorithm around the maximum of crosscorrelation. We have used a cubic spline algorithm[18], and calculated the crosscorrelation function at regular intervals spaced by $t_s/100$. The time uncertainty used in Equation (5) is therefore $t_s/100$ instead of t_s, i.e. in this case 0.05 ns. For a time delay of 500 ns, this gives a precision of 0.01%, assuming that the error on the thickness measurement and other errors are negligible.

This procedure was used with the data from *Figure 7*, and the interpolated time propagation is 2878.5 ns instead of the 2880 ns, found previously, giving a longitudinal velocity of 4214.6 ms^{-1} with a theoretical precision calculated from Equation (5) of 0.02%, mostly limited by the uncertainty of the thickness measurement. The procedure has also been applied to the data from *Figure 8*. The interpolated results are plotted in the same figure (black dots) and they show clearly the precision enhancement provided by the interpolation algorithm. From the fluctuation of the data points around a fitted smooth curve the resulting precision for this specimen is evaluated to 15 ms^{-1} or 0.2%. This is much larger than the error calculated by Equation (5), but this calculation does not take into account the uncertainty caused by the finite signal-to-noise ratio, frequency bandwidth and measurement time, or the error coming from the misalignment of the generating and detecting spots.

The error, or more precisely the standard deviation e, of a time delay measurement, t, by crosscorrelation, can be estimated and is given by[19]

$$e_t^2 = \left(2T \int_0^\infty (2\pi f)^2 \frac{|\gamma(f)|^2}{1 - |\gamma(f)|^2} \, df \right)^{-1} \tag{6}$$

where T is the observation time (i.e. the duration of each selected data portion), f the frequency and $\gamma(f)$ the coherence function defined by [19]

$$|\gamma(f)|^2 = \frac{C_{ss}^2}{(C_{ss} + C_{nn})^2} \tag{7}$$

C_{ss} and C_{nn} being the power spectra of the signal and of the noise respectively. If we denote SNR as the signal-to-noise ratio, we have

$$\frac{|\gamma(f)|^2}{1 - |\gamma(f)|^2} = \frac{C_{ss}^2}{C_{nn}^2(1 + 2C_{ss}/C_{nn})} = \frac{\mathrm{SNR}^2}{1 + 2\,\mathrm{SNR}} \tag{8}$$

and the standard deviation of the time delay measurement is therefore

$$e_t^2 = \left(2T \int_0^\infty (2\pi f)^2 \frac{\mathrm{SNR}^2}{(1 + 2\,\mathrm{SNR})} \, df \right)^{-1} \tag{9}$$

Assuming that the signal and noise power spectra are constant over the band extending from f_1 to f_2, it follows

$$e_t = \left(\frac{3}{8\pi^2 T}\right)^{1/2} \frac{(1+2\,\mathrm{SNR})^{1/2}}{\mathrm{SNR}} \frac{1}{(f_2^3 - f_1^2)^{1/2}} \qquad (10)$$

Equation (10) gives the error on the time delay measurement due to the finite time observation T, the signal-to-noise ratio SNR, and the signal bandwidth. In the case of the data of *Figure 8*, $T = 0.3$ μs, $f_1 = 1$ MHz, $f_2 = 40$ MHz, and SNR ≈ 4 (12 dB), hence giving an error $e(t) \approx 1$ ns or a precision of 0.1%. To enhance the precision, either the signal-to-noise ratio or the time duration T should be increased. The use of the interpolation algorithm increases the time resolution, but the precision cannot surpass the limit given by Equations (9) or (10) fixed by the measurement parameters. In the case of the PZT ceramic, *Figure 7*, the signal-to-noise ratio is better, SNR ≈ 10 (20 dB), and because the sample is thicker the observation time T can be larger ($T = 0.5$ μs) so that the error given by Equation (10) is ≈0.5 ns, corresponding to a precision of 0.02%.

The misalignment of the generating and detecting spots must also be taken into account. Alignment of these spots is performed by looking for the minimum time delay on an oscilloscope while the generating laser beam is translated over the surface of the specimen. The uncertainty δt, which results from this procedure is estimated to ≈1 ns, in agreement with the 0.2% precision found in *Figure 8*. Generally, the proper way to evaluate this uncertainty is to systematically repeat the measurement for the same conditions. One should also note that, in practice, alignment conditions may not be maintained in the course of a long measurement because of mechanical instability of the experimental set-up and lack of pointing stability of the lasers; a precise measurement requires verification of the alignment from time to time.

Finally, as it is the case of any physical measurement, the systematic errors should be identified, evaluated and corrected from the experimental results. The frequency dependence of ultrasonic attenuation does not affect the measurement, since the propagation delay is the same for each frequency component, which has the consequence that the maximum of the crosscorrelation function occurs at the same time offset, independent of frequency. On the other hand, as it is done for conventional ultrasonics[20] the measured phase velocity should be corrected for the effect of diffraction. Ultrasonic diffraction is caused by the finite size of the source and the finite size of the receiver and is known to bring a frequency dependent time bias on the time delay measurement made with piezoelectric transducers[20]. The effect of diffraction in our case is evaluated below. Finally, if the material is dispersive, the propagation time is frequency dependent. Therefore the time crosscorrelation method described above is not directly applicable in the case of dispersive media. A frequency domain crosscorrelation technique is also presented below for the measurement of the phase velocity in dispersive media.

Calculation of the diffraction correction

The results generally used with piezoelectric generation and detection[20] are not directly applicable to the laser-ultrasonic measurement described here. First, since the detection beam is focussed onto the surface of the specimen, detection can be considered as point-like, within the range of frequencies generally detected (1 to 10 MHz). The generating spot is also often small in comparison to the ultrasonic wavelength. Finally, these classical results, which have been derived by assuming a vibrating piston, are not obviously applicable to thermoelastic laser generation, in which the generated stresses are mostly tangential to the surface. We present below a simple derivation which permits estimation of the diffraction corrections applicable to the laser-ultrasonic technique used in this work, in particular in the case of an isotropic homogeneous material. A more general calculation is out of the scope of this paper and would require more sophisticated calculations based on the Green function[21].

The geometrical parameters involved in this calculation are described by *Figure 9*. The receiving spot is assumed to be point-like on the z axis and the generating spot is given a radius, a. The stress distribution at generation is supposed to be normal in the ablation regime, dipolar and tangential in the thermoelastic regime. It is further assumed that the distribution is uniform within the generating spot. Then we have in the ablation regime

$$\sigma_{zz}(\rho) = \sigma \text{ for } \rho < a,\ \sigma_{zz}(\rho) = 0 \text{ for } \rho > a,\ \sigma_{\rho z}(\rho) = 0 \qquad (11)$$

In the thermoelastic regime it has been shown that the dipole distribution can be replaced by outward radial forces F_r distributed along the ring of radius a[21]

$$\sigma_{\rho z} = F_r \frac{\delta(\rho - a)}{2\pi\rho} \quad \text{and} \quad \sigma_{zz} = 0 \qquad (12)$$

where δ is the Dirac function. A source element ds generates at a point on the z axis a longitudinal displacement $d\vec{u}_L$ and a shear displacement $d\vec{u}_S$. Since the interferometer only detects the displacement normal to the surface, we only have to consider the projections along the z axis. Starting first with the longitudinal velocity diffraction correction, the normal force $\sigma_{zz}\,ds$ generates along the z axis in the ablation regime the normal displacement is given by[22] Equation (13)

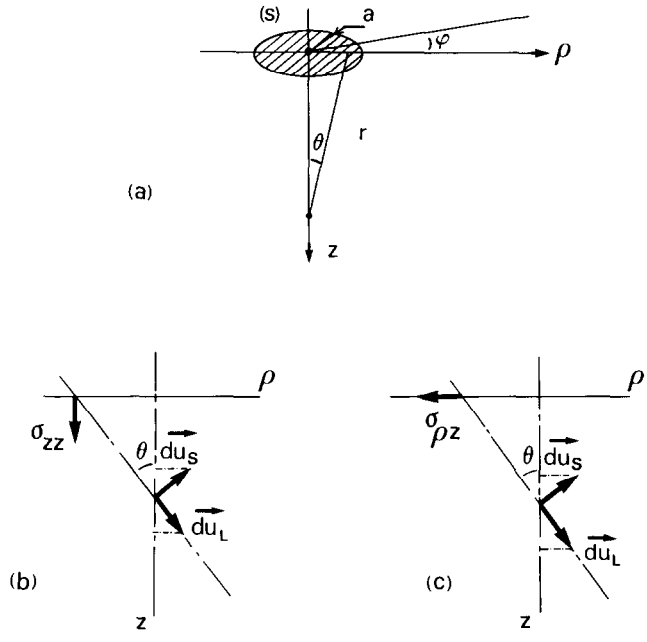

Figure 9 Geometrical parameters used in the calculation of the diffraction correction. (a) Laser generating spot and cylindrical coordinates; (b) ablation regime, normal stress; (c) thermoelastic regime, tangential stress

$$du_z = \frac{\sigma_{zz} ds}{2\pi\mu} \frac{\exp[i(\omega t - k_L r)]}{r} \frac{\cos^2\theta[(c_L/c_S)^2 - 2\sin^2\theta]}{G_0(\sin\theta)} \quad (13)$$

where λ and μ are the Lamé constants of the material, c_L and c_S are its longitudinal and shear velocities repectively, k_L is the longitudinal wave number defined by $k_L = \omega/c_L$, and $G_0(x)$ is given by

$$G_0(x) = [2x^2 - (c_L/c_S)^2]^2 - 4x^2(x^2-1)^{1/2} [x^2 - (c_L/c_S)^2]^{1/2} \quad (14)$$

In the thermoelastic regime, the radial force $\sigma_{\rho z}\, ds$ generates along the z axis the displacement du_z given by[23]

$$du_z = \frac{\sigma_{\rho z} ds}{2\pi\mu} \frac{\exp[i(\omega t - k_L r)]}{r} \times \frac{\cos\theta \sin\theta \sin 2\theta[(c_L/c_S)^2 - \sin^2\theta]^{1/2}}{G_0(\sin\theta)} \quad (15)$$

The displacement generated along the z axis by the generating spot is deduced by integration of Equations (13) and (15) over the surface, S, of the spot.

If the receiving spot is sufficiently far away ($z\lambda'/a^2 \gg 10$, λ' being the ultrasonic wavelength), we can make a parabolic approximation to a spherical wave[24], and r can be replaced by $z\,(1 + 1/2\rho^2/z^2)$ in the exponential and by z otherwise and $\sin^2\theta$ can be neglected compared with c_L/c_S. It then follows

$$u_z = \frac{\sigma}{\lambda + 2\mu} \frac{\exp[i(\omega t - k_L z)}{z} \int_0^a \exp(-ik_L\rho^2/2z)\rho\, d\rho \quad (16a)$$

in the ablation regime, and

$$u_z = \frac{F_r a^2}{\pi(\lambda + 2\mu)} \frac{\exp[i(\omega t - k_L z)}{z^3} \exp(-ik_L a^2/2z) \quad (16b)$$

in the thermoelastic regime. Integration of Equation (16a) is performed using the approximation $\exp(x) \approx 1 + x$. It then results at the first order

$$u_z = \frac{\sigma a^2}{2(\lambda + 2\mu)} \frac{\exp[i(\omega t - k_L z)]}{z} \exp(-ik_L a^2/4z) \quad (17)$$

in the ablation regime.

Equations (16b) and (17) show that the finite size of the generating spot introduces a phase shift equal to

$$\alpha \approx -\frac{k_L a^2}{4z} \text{ in the ablation regime} \quad (18a)$$

$$\alpha \approx -\frac{k_L a^2}{2z} \text{ in the thermoelastic regime} \quad (18b)$$

This gives an equivalent distance shift $\Delta z = a^2/4z$ in the ablation regime and $a^2/2z$ in the thermoelastic regime. If the velocity is determined by measuring the times of arrival t_1 and t_2 of pulses propagated over distances z_1 and z_2, its exact value is given by

$$c = \frac{(z_2 + \Delta z_2) - (z_1 + \Delta z_1)}{t_2 - t_1} = c_m\left(1 + \frac{\Delta z_2 - \Delta z_1}{z_2 - z_1}\right) \quad (19)$$

which can be written

$$c = c_m\left(1 + \frac{\Delta z_2 - \Delta z_1}{z_2 - z_1}\right) \quad (20)$$

where c_m is the measured value given by $(z_2 - z_1)/(t_2 - t_1)$. We then deduce the correction which should be applied to the measured velocity

$$\frac{\Delta c}{c} = \frac{-a^2}{4z_1 z_2} \text{ in the ablation regime} \quad (21a)$$

$$\frac{\Delta c}{c} = \frac{-a^2}{2z_1 z_2} \text{ in the thermoelastic regime} \quad (21b)$$

The correction is negative, and the values $a^2/4z_1z_2$ and $a^2/2z_1z_2$ should be subtracted from those deduced from the time delay measurement. Equation (21a) is twice the result obtained for a piston source in the spherical wave approximation with a receiver of same diameter[24]. We also note that, the correction is independent of frequency. This has the consequence that the correlation maximum is equally shifted for all the frequencies. This situation does not generally occur in practice with piezoelectric generation and detection, since the sizes of transducers and specimens typically encountered mean that the spherical wave approximation conditions are rarely satisfied, resulting in frequency dependent corrections.

In the case of the diffraction corrections applicable to the shear velocity measurement, we should instead consider the projection du'_z along the z axis of the shear displacement $d\vec{u}_S$. In the ablation regime, the normal force $\sigma_{zz}\, ds$ generates along the z axis the displacement du'_z given by[22]

$$du'_z = \frac{\sigma_{zz} ds}{2\pi\mu} \frac{\exp[i(\omega t - k_S r)]}{r} \times \frac{\sin\theta \sin 2\theta[(c_L/c_S)^2 \sin^2\theta - 1]^{1/2}}{G_0[(c_L/c_S)\sin\theta]} \left(\frac{c_L}{c_S}\right)^3 \quad (22)$$

and in the thermoelastic regime, the radial force $\sigma_{\rho z}\, ds$ generates along the z axis the radial displacement du'_z given by[23]

$$du'_z = \frac{\sigma_{\rho z} ds}{2\pi\mu} \frac{\exp[i(\omega t - k_S r)]}{r} \frac{\sin\theta \sin 4\theta}{G_0[(c_L/c_S)\sin\theta]} \left(\frac{c_L}{c_S}\right)^3 \quad (23)$$

Using the same procedure as above, the following relative diffraction corrections to be applied to the shear velocity are derived

$$\frac{\Delta c}{c} = \frac{-a^2}{3z_1 z_2} \text{ in the ablation regime} \quad (24a)$$

$$\frac{\Delta c}{c} = \frac{-a^2}{2z_1 z_2} \text{ in the thermoelastic regime} \quad (24b)$$

Equation (21b) has been applied to the data, from the PZT ceramic in *Figure 7*, giving a correction error of -0.03% or $-1.2\ \text{ms}^{-1}$. This correction is of the order of the error resulting from the time and thickness meaurements uncertainties, and therefore must be made. In other cases where the errors on time delay and thickness are much larger, the diffraction correction would be negligible.

Time delay measurement in a dispersive medium

In a dispersive material, the phase velocity is frequency dependent, and the shape of the ultrasonic pulses is modified as they propagate inside the material. The crosscorrelation method described above has been applied

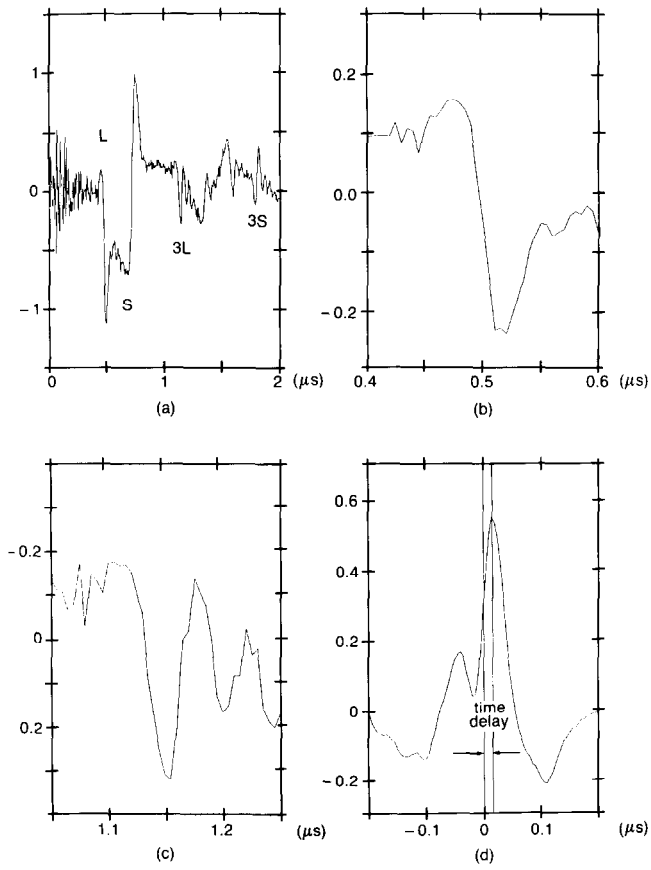

Figure 10 Crosscorrelation measurement of time arrival in the Al_2O_3-Al-SiC (No. 1) sample of *Figure 2*. (a) Epicentral particle velocity (derivative of the epicentral displacement of *Figure 2*); (b) normalized and d.c. corrected L arrival (window 0.4–0.6 μs); (c) normalized and d.c. corrected $3L$ arrival (1.05 – 1.25 μs); (d) crosscorrelation of the two windows in (b) and (c). The coarse delay is 1.050 – 0.400 = 0.650 μs. The fine delay is 0.016 μs (maximum + interpolation), propagation time: $t_{2L} = 0.634$ μs

to the data of the Al_2O_3-Al-SiC (No. 1) ceramic–metal composite, shown in *Figure 2*. The selected data portions for longitudinal velocity determination and the crosscorrelation function are shown in *Figure 10*. It can be readily seen that the shapes of the L and $3L$ pulses are very different, which denotes ultrasonic dispersion in the material. The time delay measured at the maximum of the crosscorrelation represents some mean value of the propagation time within the frequency band. To extract the frequency dependent time propagation, a frequency approach is more suited. A frequency crosscorrelation technique is described below, which allows determination of the phase velocity dispersion in the material.

The Fourier transform $C_{uv}(f)$ of the crosscorrelation of two signals $u(t)$ and $v(t)$ can be expressed as a function of their Fourier transforms $U(f)$ and $V(f)$ by

$$C_{uv}(f) = U(f) \cdot V^*(f) \tag{25}$$

where * means complex conjugate. If $u(t)$ and $v(t)$ represent the same ultrasonic pulse at distances z_1 and z_2, respectively, $U(f)$ and $V(f)$ can be expressed as follows

$$U(f) = M(f) \exp[iP(f)] \exp[i2\pi f\, z_1/c(f)] \tag{26a}$$

$$V(f) = M(f) \exp[iP(f)] \exp[i2\pi f\, z_2/c(f)] \tag{26b}$$

where $M(f)$ and $P(f)$ are the amplitude and phase of the ultrasonic generated pulse, respectively, and $c(f)$ is the frequency dependent ultrasonic velocity. The Fourier transform of the crosscorrelation can therefore be written

$$C_{uv}(f) = M^2(f) \exp[i2\pi f(z_2 - z_1)/c(f)] \tag{27}$$

Equation (27) shows that the phase $\psi(f)$ of the Fourier transform of the crosscorrelation is directly related to the frequency dependent propagation time $t(f)$ and to the phase velocity $c(f)$

$$t(f) = \frac{\psi(f)}{2\pi f} = \frac{z_2 - z_1}{c(f)} \tag{28}$$

The procedure to measure the phase velocity dispersion is illustrated in *Figure 11* using the data from *Figure 10*. First the two successive echoes L and $3L$ of *Figures 10b* and *c* are selected with a Blackmann-Harris window[25], and represented in *Figure 11a*. Windowing is necessary to minimize the effect of the time truncation on the frequency spectrum. Crosscorrelation of the two selected data portions is calculated as previously and then Fourier transformed. The phase of the Fourier transform of the crosscorrelation is given in *Figure 11b*. This phase appears as a linear function of frequency, as should be expected, this corresponds simply to a delay between the two pulses.

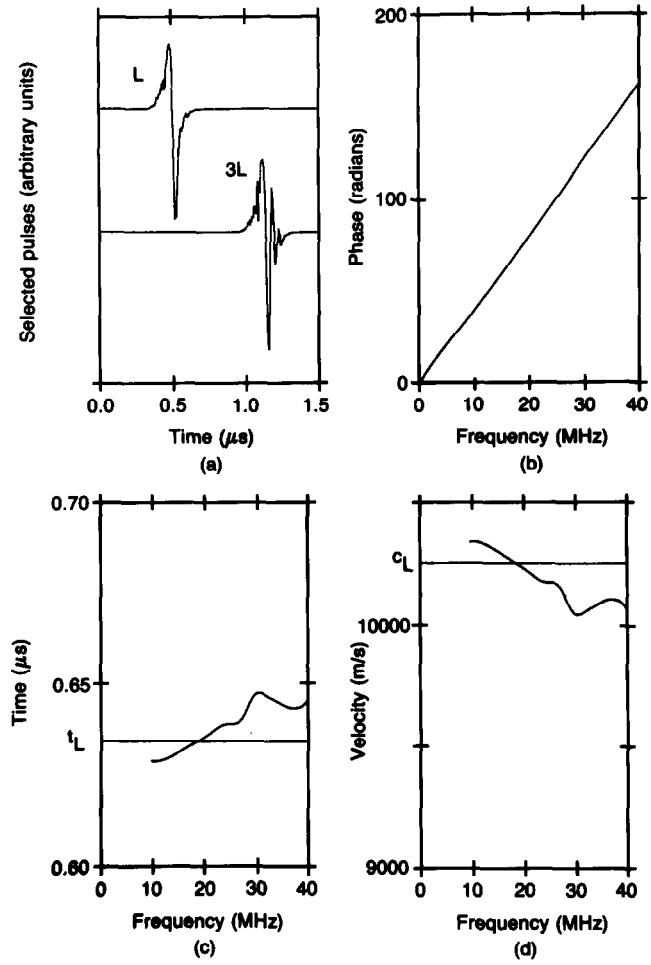

Figure 11 Phase velocity dispersion measurement in the Al_2O_3-Al-SiC (No. 1) composite of *Figure 2* and *10*. (a) Normalized and windowed L and $3L$ arrivals; (b) phase of the Fourier transform of the crosscorrelation of the two echoes; (c) longitudinal propagation time from the phase of the crosscorrelation, t_L is the time delay measured by crosscorrelation; (d) longitudinal velocity from the propagation time, c_L is the velocity measured by crosscorrelation

The calculation of the time delay using Equation (28) shows that this is not exactly true and that dispersion occurs. The time delay is plotted in *Figure 11c*. From the frequency dependent propagation time $t(f)$, the phase velocity is derived by Equation (28), and is represented in *Figure 11d*. The phase velocity dispersion for this example is approximately 2% for frequencies up to 35 MHz.

The precision of the phase velocity dispersion determination can be estimated as done previously for crosscorrelation in terms of signal-to-noise ratio and measurement time. The lower frequency limit depends on the window duration T and is given by $f_m = 1/T$. The standard deviation e_ψ on the phase is expressed by[26]

$$e_\psi^2(f) = \frac{1 - |\gamma(f)|^2}{2|\gamma(f)|^2} \tag{29}$$

$\gamma(f)$ being the coherence function defined above. The standard deviation, e_t, of the propagation time at the frequency f follows from Equations (28) and (29)

$$e_t^2(f) = \frac{1}{(2\pi f)^2} \frac{1 - |\gamma(f)|^2}{2|\gamma(f)|^2} \tag{30}$$

If the material is non dispersive, the propagation time can be deduced from phase data by a regression analysis, which yields the same uncertainty as given previously by Equation (9)[25]. This means that for a non-dispersive material, time or frequency crosscorrelation analysis have the same precision. If the material is dispersive, the propagation time is frequency dependent and the standard deviation at a frequency f is given using Equations (8) and (30) by

$$e_t(f) = \frac{1}{2\pi f} \frac{(1 + 2\,\mathrm{SNR}(f))^{1/2}}{(2)^{1/2}\,\mathrm{SNR}(f)} \tag{31}$$

For the data from *Figure 11*, the observation time is $T = 0.5$ μs and the signal-to-noise ratio is estimated to SNR = 25 (28 dB) in the frequency band of the signal. Equation (31) then yields the error $e_t(f) = 0.032/f$ (μs), f being expressed in MHz. This shows that precision diminishes towards low frequencies. In the case of the example given, the valid portion starts above 8 MHz. The oscillations above 25 MHz are caused by decreasing signal-to-noise ratio at high frequencies. The propagation time and the phase velocity measured previously by the crosscorrelation technique are denoted t_L and c_L in *Figure 11*, and correspond to some mean value in the frequency range. This value of c_L is not generally the one which should be used in the calculation of the elastic constants.

Elastic constants determination from velocities

In the case of an isotropic material, the elastic constants (either bulk modulus B and shear modulus G, or Young's modulus E and Poisson's ratio ν, or Lame constants λ and μ) can be readily deduced from the longitudinal c_L and shear c_S ultrasonic velocities and density ρ using well-known equations, shown below:

$$B = \rho\left(c_L^2 - \frac{4}{3}c_S^2\right), \quad G = \rho c_S^2 \tag{32a}$$

$$E = \rho c_S^2 \frac{(3c_L^2 - 4c_S^2)}{(c_L^2 - c_S^2)}, \quad \nu = 0.5\left(1 - \frac{c_S^2}{(c_L^2 - c_S^2)}\right) \tag{32b}$$

$$\lambda = \rho(c_L^2 - 2c_S^2), \quad \mu = \rho c_S^2 \tag{32c}$$

However, some difficulties may occur when the material is dispersive since the values of velocities used in the above formulae are the asymptotic values at low frequencies, which may not be easily derived from the laser-ultrasonic measurement. As is seen in *Figure 11*, it may not be possible to directly measure velocities at low ultrasonic frequencies, so the asymptotic value should be extrapolated from data available at higher frequencies. In such circumstances, some theoretical knowledge concerning the origin of dispersion and its variation with frequency is useful. Dispersion may be caused by inelasticity of the material or scattering by its microstructure[27]. In the case of the material used in *Figure 11*, dispersion is mainly caused by scattering, so we should expect the velocity to be constant up to some value and then to vary monotically[28]. Such a trend is consistent with the variation observed in *Figure 11d*, where a plateau appears to be reached at ≈10 MHz, giving a value of 10300 ms^{-1}. Therefore, this velocity should be taken as the asymptotic value to be used in Equation (32). A thicker sample, if it had been available would have permitted a wider truncation and therefore reached lower frequencies, but the noise would have been larger, so improvement would not have been guaranteed.

The difficulties encountered with this sample are typical. Worse cases can even be encountered when higher noise makes this frequency analysis impossible, which leaves only the result of the simple crosscorrelation. In this case, accuracy may be limited by dispersion to a few per cent. This accuracy level is sufficient for engineering purposes, in many cases involving advanced composite materials.

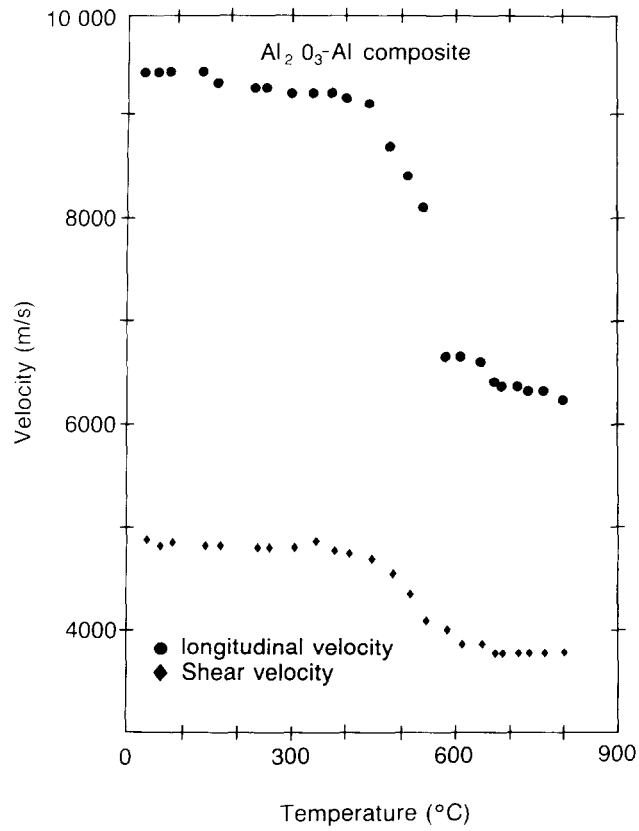

Figure 12 Ultrasonic velocities vs temperature for an Al_2O_3-Al ceramic–metal composite. The step around 500–600 °C corresponds to the aluminium melting temperature

Other difficulties for the determination of the elastic constants from the velocities occur when Equation (32) are not applicable, in particular when the material includes molten metal. Such a case is illustrated in *Figure 12*. These data also include a plot of the shear velocity, which was obtained by the crosscorrelation and interpolation technique. Although in all the examples given previously the longitudinal velocity is measured, all the techniques described here are equally applicable to shear wave velocity determination. The drop in velocities around 500–600°C is caused by melting of the aluminium contained in the ceramic skeleton. Below 500°C, Equations (32) can be applied to determine the elastic constants. Above aluminium melting, these equations are not applicable and a propagation model including the liquid phase should be used to derive the relations between the elastic constants and the measured velocities.

Assuming that there is no fundamental difficulty in determining the elastic constants from the velocities, one obvious way to test the accuracy of this technique is to compare its results with those obtained by conventional techniques. This was done, as explained below, for single crystal germanium, a nondispersive material in the considered frequency range. This measurement is also, to our knowledge, the first measurement of elastic constants of an anisotropic material by laser-ultrasonics, although the ultrasonic velocity of anisotropic metallic glasses has already been studied using laser-generated and piezoelectrically detected ultrasonic waves[29].

Laser-ultrasonic determination of the elastic constants of single crystal germanium

Germanium single crystals have cubic symmetry. If we denote ⟨100⟩, ⟨010⟩ and ⟨001⟩ the normals to the cube's face and take them as cartesian references, the elastic constant tensor $[c]$ can be written

$$[c] = \begin{vmatrix} c_{11} & c_{12} & c_{12} & 0 & 0 & 0 \\ c_{12} & c_{11} & c_{12} & 0 & 0 & 0 \\ c_{12} & c_{12} & c_{11} & 0 & 0 & 0 \\ 0 & 0 & 0 & c_{44} & 0 & 0 \\ 0 & 0 & 0 & 0 & c_{44} & 0 \\ 0 & 0 & 0 & 0 & 0 & c_{44} \end{vmatrix} \quad (33)$$

c_{11}, c_{12}, c_{44} being the three independent constants. For any direction, three types of waves can propagate: a quasi-longitudinal wave, and two quasi-shear waves. The velocities of these waves can be expressed as a function of c_{11}, c_{12}, c_{44} and of the density ρ. *Table 2* gives the expressions of longitudinal and shear velocities in the ⟨100⟩, ⟨110⟩ and ⟨111⟩ directions. The measurement of three different velocities that are related to c_{11}, c_{12}, c_{44} by independent relations will permit the determination of the three elastic constants.

The laser-generated normal displacement waveforms measured at room temperature (25°C) at the epicentre of specimens cut in ⟨100⟩, ⟨110⟩ and ⟨111⟩ directions are shown in *Figure 13*. In the ⟨100⟩ and ⟨111⟩ directions, the shear and quasi-shear velocities are identical and are denoted *S*. In the ⟨110⟩ direction, the shear and quasi-shear velocities are different and noted respectively *S*1 and *S*2. As for an isotropic material, unambiguous identification of the arrival times is a prerequisite to any velocity measurement. Identification from comparison to the theoretical waveforms of *Figures 4, 5* and *6* is impossible, since germanium is anisotropic of cubic symmetry. Calculation of the theoretical waveforms is out of the scope of this paper and would require calculation of the Green function for a material of cubic symmetry. The arrival times of the various ultrasonic waves have consequently been identified using experimental values of the velocities taken in the literature[30,31].

Once the arrival times have been identified, and following observation of the expressions given in *Table 2*, we have chosen to measure longitudinal velocities in ⟨111⟩ and ⟨100⟩ directions, and shear velocity in ⟨100⟩ direction to determine the three elastic constants (the

Table 2 Relations between elastic constants and sound velocities for a material of cubic symmetry

Direction of propagation	Direction of particle motion	Type of wave	Velocity
⟨100⟩	⟨100⟩	Longitudinal	$C_L = (c_{11}/\rho)^{1/2}$
⟨100⟩	in plane (100)	Shear (*S*)	$C_S = (c_{44}/\rho)^{1/2}$
⟨110⟩	⟨110⟩	Longitudinal	$C_L = \left(\frac{c_{11}+c_{12}+2c_{44}}{2\rho}\right)^{1/2}$
⟨110⟩	⟨001⟩	Shear (*S*1)	$C_S = (c_{44}/\rho)^{1/2}$
⟨110⟩	⟨$\overline{110}$⟩	Shear (*S*2)	$C_S = \left(\frac{c_{11}-c_{12}}{2\rho}\right)^{1/2}$
⟨111⟩	⟨111⟩	Longitudinal	$C_L = \left(\frac{c_{11}+2c_{12}+4c_{44}}{3\rho}\right)^{1/2}$
⟨111⟩	in plane (111)	Shear (*S*)	$C_S = \left(\frac{c^{11}-c^{12}+c^{44}}{3\rho}\right)^{1/2}$

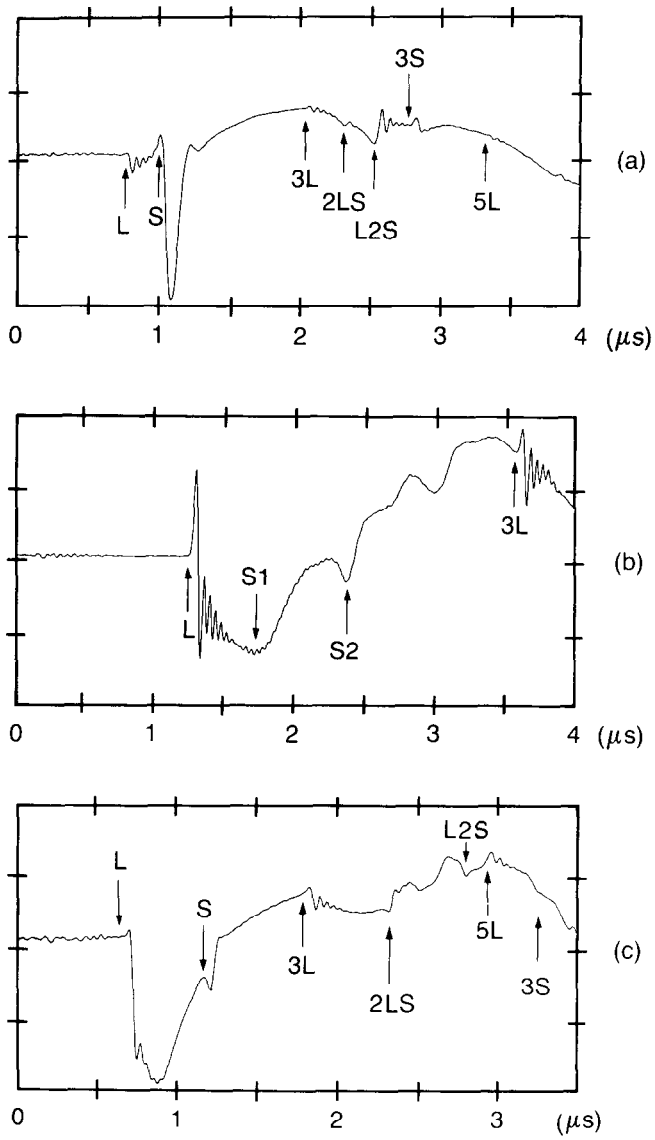

Figure 13 Laser-generated displacements measured at epicentre on single crystals germanium specimens. (a) ⟨100⟩ direction, thickness 3.167 mm; (b) ⟨110⟩ direction, thickness 6.380 mm; (c) ⟨111⟩ direction, thickness 3.132 mm

longitudinal velocity in the ⟨110⟩ direction could have been used as well). The following relations are then used

$$c_{11} = \rho c_L^2\langle 100\rangle$$
$$c_{44} = \rho c_S^2\langle 100\rangle \qquad (34)$$
$$c_{12} = 0.5\rho(3c_L^2\langle 111\rangle - c_L^2\langle 100\rangle - 4c_S^2\langle 100\rangle)$$

The velocities are determined by derivation, cross-correlation of consecutive echoes and cubic spline interpolation, using the data from *Figure 13*. The results corrected from diffraction are shown in *Table 3*, and the elastic constants calculated by Equation (34) are listed in *Table 4*. *Tables 3* and *4* include for comparison values taken from the literature measured by contact pulse-echo[30] and resonance[31] methods. Our results are very close to the references: 0.3% difference on $c_L\langle 111\rangle$, 0.3% on $c_L\langle 100\rangle$ and 0.7% on $c_S\langle 100\rangle$ with reference 30, and 0.3% on $c_L\langle 111\rangle$, 0.4% on $c_L\langle 100\rangle$ and 0.4% on $c_S\langle 100\rangle$ with reference 31.

Our measurement errors are estimated as above and are indicated in *Table 1*. They are mostly associated with

Table 3 Sound velocities in germanium at 25°C

Units (ms^{-1})	C_L ⟨111⟩	C_L ⟨100⟩	C_S ⟨100⟩	Density ($Kg\,m^{-3}$)
Contact pulse-echo method[30]	5561	4921	3550	5323
Resonance method[31]	5587	4959	3536	5350
Laser-ultrasonics (measured)	5577	4937	3522	5323

Table 4 Elastic constants of germanium at 25°C

Units (Nm^{-2})	c_{11}	c_{12}	c_{44}
Contact pulse-echo method[30]	1.289	0.483	0.671
Resonance method[31]	1.316	0.509	0.669
Laser-ultrasonics (calculated from data of *Table 3*)	1.297	0.514	0.660

laser misalignment and the thickness measurements. The phase velocity dispersion meaured by the frequency crosscorrelation technique is negligible as expected (below 0.01%). It must be noted that the two conventional methods have differences of 0.5% on $c_L\langle 111\rangle$, 1.0% on $c_L\langle 100\rangle$ and 0.5% on $c_S\langle 100\rangle$. Furthermore using a resonance method with an estimated precision of 0.06%, an average scatter of 0.2% of the elastic moduli was found on different samples of same orientation[32]. In conclusion, the values obtained for germanium single crystal are in good agreement with previous measurements and have similar accuracy.

Conclusion

A method to measure material elastic constants based on laser-ultrasonic generation and detection has been presented. This method has all the advantages of laser-ultrasonics over classical methods. In particular it is noncontact and permits measurement at elevated temperatures. The problems of buffer rods, bonds, momentary contact and cooling of the conventional pulse-echo techniques are thus eliminated. The specimen shape is not critical, as it is in the case for classical pulse-echo and resonance methods, and the measurements can be readily performed on curved surfaces, as shown in *Figures 8* and *12*. Furthermore in this technique both longitudinal and shear velocities are measured simultaneously, eliminating the mounting and dismounting of different transducers of the conventional technique.

In the method presented, ultrasound is generated by the thermoelastic effect, with in the cases of poor signal-to-noise ratio a very slight ablation, so that sufficiently marked longitudinal and shear features are observed. No serious damage to the sample occurs, so that unlimited probing at the same location and signal averaging is possible. Ultrasound velocities are measured by crosscorrelation of consecutive echoes and reliable and reproducible results are obtained, even with poor signal-to-noise ratios. Precision is further enhanced by data interpolation, so the uncertainty introduced by the sampling time is typically reduced to a value of 0.01%. This

precision level can only be reached for sufficiently thick samples and good signal-to-noise ratios. In the other cases, the limited sampling window, limited bandwidth and noise level decrease the precision and a value of the order of 0.1% is more typical. The highest precision level is reached when one measures the variation of velocity caused by a changing external parameter over a short time base. Over a long time base, precision is further limited by laser spot alignment and laser pointing stability, giving an uncertainty of the order of 0.1%. The systematic error caused by diffraction has been evaluated and is often negligible for sufficiently thick samples. We have shown that dispersion effects can be evaluated by frequency analysis of the crosscorrelation function when the signal-to-noise ratio is sufficient. In this case, the absolute accuracy could be of the order of 0.1%, otherwise dispersion may be the limiting factor, since crosscorrelation provides only some mean velocity value. We have discussed how the elastic constants can be deduced from the measurement of the velocities and how various difficulties occur with dispersive samples and others. The absolute accuracy of the method has been tested by comparing the results obtained on germanium single crystal with known data obtained by classical pulse-echo and resonance methods. The laser-ultrasonics method used is judged to be as accurate as these classical methods.

Acknowledgements

The authors thank Dr N. N. Hsu for providing the computer program used to generate theoretical data, Dr A. J. Gesing and G. Burger of Alcan International for several aluminium based ceramic composites, R. Beauprie of Cominco Ltd for the single crystal germanium samples, as well as Dr C. K. Jen for useful discussions and R. Héon for his technical support during the course of this work.

References

1 **McSkimin, H.J.** Ultrasonic methods for measuring the mechanical properties of liquids and solids, in: *Physical Acoustics* Vol. 1A (Ed. Mason, P.) Academic Press (1964) Chapter 4, 271–334

2 **Schreiber, E., Anderson, O. and Soga, N.** *Elastic constants and their measurement* McGraw-Hill, New York (1973)

3 **Dunegan, H.L.** High temperature dynamic modulus measurement by use of ultrasonics *Materials Evaluation* (1964) **22**, 266–272

4 **Papadakis, E.P., Lynnworth, L.C., Fowler, K.A. and Carnevale, E.H.** Ultrasonic attenuation and velocity in hot specimens by the momentary contact method with pressure coupling and some results on steel to 1200°C, *J. Acous. Soc. Am* (1972) **52** 850–857

5 **Burenkov, Y.A. and Nikanorov, S.P.** Elastic properties and binding forces in crystals with diamond and sphalerite lattices *Soviet Phys. Solid State*, (1984) **26 (11)** 1940–1944

6 **Scruby, C.B., Dewhurst, R.J. and Hutchins, D.A. and Palmer, S.B.** Laser generation of ultrasound in metals in: *Research Techniques in NDT*, Vol. 5, (Ed. Sharpe, R.S.) Academic Press, New York (1982) 281–327

7 **Monchalin, J.-P.** Optical detection of ultrasound, *IEEE Trans. Ult., Ferroelec. Frequency Control*, (1986) **UFFC-33** (5) 485–499

8 **Calder, C.A., Draney, E.C. and Wilcox, W.W.** Noncontact measurement of the elastic constants of plutonium at elevated temperature *J. Nucl. Mater.* (1981) **97** 126–136

9 **Dewhurst, R.J., Edwards, C., Mckie, A.D.W. and Palmer, S.B.** A remote laser system for ultrasonic velocity measurement at high temperatures *J. Appl. Phys.* (1988) **63** 1225–1227

10 **Bresse, L.F., Hutchins, D.A. and Lundgren, K.** Elastic constants determination using ultrasonic generation by pulsed lasers, *Rev. Prog. Quant. NDE* (1987) June 21–26 Williamsburg, VA

11 **Monchalin, J.-P., Héon, R., Bussière, J.F. and Farahbakhsh, B.** Laser-ultrasonic determination of elastic constants at ambient and elevated temperatures, in *Nondestructive Characterization of Materials II* (Ed Bussière, J.F., Monchalin, J.-P., Ruud, C.O. and Green, R.E. Jr.) Plenum Publishing, USA (1987) 717–723

12 **Piché, L., Champagne, B. and Monchalin, J.-P.** Laser ultrasonics measurements of elastic constants of composites *Mater. Eval.* (1987) **45** 74–79

13 **Monchalin, J.-P., Héon, R. and Muzak, N.** Evaluation of ultrasonic inspection procedures by field mapping with an optical probe *Canad. Metallurg. Quar.* (1986) **25** 247–252

14 **Monchalin, J.-P., Héon, R. and Muzak, N.** Heterodyne interferometric laser probe to measure continuous ultrasonic displacements. *Rev. Sci. Instrument.* (1985) **56** 543–546

15 **Rose, L.R.F.** Point-source representation for laser-generated ultrasound, *J. Acoust. Soc. Am.* (1984) **75** (3) 723–732

16 **Hsu, N.H.** Dynamic Green's function of an infinite plate, A computer program *Report NBSIR 85-3234* National Bureau of Standards, Gaithersburg, MD (1985)

17 **Hull, D.R., Kautz, H.E. and Vary, A.** Measurement of ultrasonic velocity using phase-slope and crosscorrelation methods *Mater. Eval.* (1985) **43** 1455–1460

18 **Press, W.H., Flannery, B.P., Teukolsky, S.A. and Vetterling, W.T.** *Numerical recipes: the art of scientific computing* Cambridge University Press, Cambridge, UK (1986) Chapter 3, 86–89

19 **Quazi, A.H.** An overview on the time delay estimate in active and passive systems for target localization, *IEEE Trans Acoust. Speech Signal Process.* (1981) **ASSP-29 No 3** 527–533

20 **Papadakis, E.P.** Ultrasonic diffraction from single apertures with application to pulse measurements and crystal physics in: *Physical Acoustics* Vol. 11 Academic Press, New York (1975) Chapter 3 151–211

21 **Bresse, L.F. and Hutchins, D.A.** Transient generation of elastic waves in solids by wide sources. *J. Acoust. Soc. Am.* (submitted)

22 **Lord, A.E.** Geometric diffraction loss in longitudinal and shear wave attenuation measurements in an isotropic half-space, *J. Acoust. Soc. Am.* (1966) **39**(4) 650–662

23 **Aussel, J.-D.** Génération par laser d'ondes ultrasonores dans les matériaux – Application au Contrôle Non-Destructif *Thèse de doctorat* INSA Lyon (France) #86ISAL0018 (1986)

24 **Khimunin, A.S.** Numerical calculation of the diffraction corrections for the precise measurement of ultrasound phase velocity *Acoustica* (1975) **32** 192–200

25 **Harris, F.J.** On the use of windows for harmonic analysis with the discrete Fourier transform *Proc. IEEE* (1978) **66** 51–83

26 **Piersol, A.G.** Time delay estimation using phase data *IEEE Trans. Acoust., Speech Signal Process.* (1981) **ASSP-29**(3) 471–477

27 **Truell, R., Elbaum, C. and Chick, B.B.** *Ultrasonic methods in solid state physics* Academic Press, New York (1969)

28 **Stanke, F.E. and Kino, G.S.** A unified theory for elastic wave propagation in polycrystalline materials *J. Acoust. Soc. Am.* (1984) **75**(2) 665–681

29 **Rosen, M., Wadley, H.N.G. and Mehrabian, R.** Crystallization kinetic study of amorphous Pd-Cu-Si by ultrasonic measurements *Scripta Metallurgica* (1981) **15** 1231–1236

30 **McSkimin, H.J.** Measurement of ultrasonic wave velocities and elastic moduli for small solid specimens at high temperature *J. Acoust. Soc. Am.* (1959) **31**(3) 287–295

31 **Hearmon, R.F.S.** The elastic constants of anisotropic materials *Advanced Physics* (1956) **5** 323–382

32 **Burenkov, Yu. A., Nikanorov, S.P. and Stepanov, A.V.** Elastic properties of Germanium *Sov. Phys. Solid State*, (1971) **12**(8) 1940–1942